ACI STRUCTURAL JOURNAL TECHNICAL PAPER

Title no. 100-S4

# Deformation Behavior of Fiber-Reinforced Polymer Reinforced Engineered Cementitious Composite (ECC) Flexural Members under Reversed Cyclic Loading Conditions

by Gregor Fischer and Victor C. Li

*This study investigates the response of fiber-reinforced polymer (FRP) reinforced engineered cementitious composite (ECC) members with a focus on their flexural load-deformation behavior, residual deflection, damage evolution, and failure mode. Critical aspects of conventional FRP-reinforced concrete members—such as interfacial bond strength, flexural crack formation, composite deformation behavior, and brittle failure mode—are briefly reviewed and compared to FRP reinforced ECC. The interaction of linear elastic FRP reinforcement and ECC matrix with ductile stress-strain behavior in tension results in nonlinear elastic flexural response characteristics with stable hysteretic behavior, small residual deflection, and ultimately gradual compression failure. Compatible deformations of reinforcement and matrix lead to low interfacial bond stress and prevent composite disintegration by bond splitting and cover spalling. Furthermore, flexural stiffness and strength as well as crack formation and widths in FRP-reinforced ECC members are found effectively independent of interfacial bond properties due to the tensile deformation characteristics of the cementitious matrix. A model for the load-deflection envelope based on a nonlinear moment-curvature relationship is suggested.*

**Keywords**: bond; composite; deformation; reinforcement; tolerance.

## INTRODUCTION

Besides strengthening and retrofitting existing structures with FRP sheets, most research activities on fiber-reinforced polymer (FRP) reinforced concrete have been substantiated by the corrosion resistance of FRP reinforcement (ACI Committee 440 1996; Taerwe 1995). These studies mainly focused on investigating the structural properties of FRP-reinforced concrete, particularly flexural strength, ductility (Naaman and Jeong 1995; Harris, Samboonsong, and Ko 1998) and failure mode (Nanni 1993; Yost, Goodspeed, and Schmeckpeper 2001), interfacial bond characteristics (Burgoyne 1993; Cosenza, Manfredi, and Realfonzo 1997; Focacci, Nanni, and Bakis 2000; Katz 2000), crack width (Theriault and Benmokrane 1998), and the prediction of the moment-deflection relationship (Benmokrane, Chaalal, and Masmoudi 1995; Pecce, Manfredi, and Cosenza 2000; Alsayed 1998; Razaqpur, Švecová, and Cheung 2000).

The flexural load-deformation behavior of FRP-reinforced concrete members is characterized by a lower flexural stiffness at a given reinforcement ratio compared to steel reinforced members (ACI Committee 440 1996). This difference results from a significantly lower modulus of elasticity of most FRP-reinforcement materials compared with conventional steel reinforcement, particularly those using glass and aramid fibers with composite elastic moduli of approximately 40 and 60 GPa, respectively. To meet serviceability requirements, deflections of FRP-reinforced concrete members can be effectively reduced by increasing either the FRP reinforcement ratio (Theriault and Benmokrane 1998; Pecce, Manfredi, and Cosenza 2000; Yost, Goodspeed, and Schmeckpeper 2001) or cross-sectional dimensions of the member (Fukuyama et al. 1995; Alsayed 1998).

Interfacial bond characteristics strongly influence the behavior of FRP-reinforced concrete with respect to member deflection, crack spacing, and width (Tighiouart, Benmokrane, and Gao 1998; Cosenza, Manfredi, and Realfonzo 1997). Bond failure may occur either by interface delamination due to insufficient shear strength between reinforcing bar core and attached surface deformations (Katz 2000) or by longitudinal splitting of concrete surrounding the reinforcing bar (Ye and Wu 2000), which essentially eliminates mechanical interaction between matrix and reinforcement (Guo and Cox 2000). Sand coating of FRP reinforcement, in addition to a deformed surface geometry, has been found to provide high interfacial bond strength (Cosenza, Manfredi, and Realfonzo 1997), which, however, increases the tendency of bond splitting (Nanni and Taginaki 1992). In contrast, studies on prestressed FRP concrete members suggest the use of partially debonded FRP reinforcement to increase the member deflection capacity (Lees and Burgoyne 1999) and allow reinforcement strain redistribution over an extended length in the vicinity of a flexural crack (Nanni 1993).

It has been recognized that FRP-reinforced concrete members possess insufficient ductility due to the material properties of the longitudinal reinforcement (ACI Committee 440 1996). Concepts to overcome this deficiency include ductile compression failure of concrete by providing confinement reinforcement or using fiber-reinforced concrete (Naaman and Jeong 1995; Alsayed and Alhozaimy 1999) as well as hybrid FRP reinforcement with inherent ductility (Harris, Samboonsong, and Ko 1998). These concepts may provide a more gradual failure mode under monotonic loading conditions as compared to tensile failure of FRP reinforcement. Under reverse cyclic loading conditions, however, they are unable to maintain their energy dissipation capabilities due to the unrepeatable nature of their inelastic deformation mechanism, that is, concrete crushing, fiber pullout, or partial tendon rupture.

*ACI Structural Journal*, V. 100, No. 1, January-February 2003.
MS No. 01-310 received September 30, 2001, and reviewed under Institute publication policies.  Pertinent discussion will be published in the November-December 2003 *ACI Structural Journal* if received by July 1, 2003.

**Gregor Fischer** *is an assistant professor in the Department of Civil and Environmental Engineering at the University of Hawaii at Manoa. He received his PhD and MSE from the University of Michigan, Ann Arbor, Mich. His research interests include the design of fiber-reinforced cement composites and their structural applications.*

**Victor C. Li** *is a professor in the Department of Civil and Environmental Engineering at the University of Michigan. His research interests include micromechanics-based design of fiber-reinforced cementitious composites and integrated materials-structural design for performance enhancement, including repair and retrofit of infrastructures.*

Analytical models based on fundamental concepts of force equilibrium and compatibility have been successfully applied to predict the ultimate flexural strength of FRP-reinforced concrete members (ACI Committee 440 1996; Pecce, Manfredi, and Cosenza 2000; Yost, Goodspeed, and Schmeckpeper 2001). Flexural deformations under service and ultimate conditions, however, are commonly found to be underpredicted by the equations recommended in current design guidelines that were originally developed for steel-reinforced members and do not explicitly account for the elastic modulus of the reinforcement (ACI Committee 440 1996; Sonobe, Fukuyama, and Okamoto 1997). Therefore, modifications to this model have been suggested, employing correlation coefficients based on experimentally obtained data (Benmokrane et al. 1997). In another approach, the curvature distribution along an arbitrary flexural member was taken into consideration to arrive at a more generally applicable moment-deflection model (Razaqpur, Švecová, and Cheung 2000).

Particular flexural members in seismic resistant structures such as beams and first-story columns may be required to undergo relatively large flexural deformations while maintaining their load-carrying capacity. In steel-reinforced concrete members, these deformations are likely to exceed the elastic deflection limit, which accommodates the need for energy dissipation; however, it also implies relatively large residual deformations after unloading. To provide the structure with self-centering capabilities after experiencing large, nonlinear deformations, unbonded post-tensioned steel tendons may be employed in various types of construction, such as precast concrete (Priestley, Sritharan, and Conley 1999; El-Sheikh, Sause, and Pessiki 1999; Kurama, Pessiki, and Sause 1999) and steel structures (Ricles, Sause, and Garlock 2001). Although these steel tendons usually have a larger elastic strain limit compared to mild steel reinforcement, it is still necessary to distribute their elongation over an extended length to avoid yielding and consequently unbonded reinforcement is required.

A large-scale experimental investigation was conducted on the structural performance of FRP-reinforced concrete members in a moment resisting frame (Fukuyama et al. 1995). According to this study, the load-deformation behavior of the frame showed small residual deflections after unloading as well as a stable hysteresis until crushing of the concrete at 2% drift. Due to small residual deformations, rehabilitation of the structure was presumed to involve relatively little effort and a relaxation of the maximum deflection limit was suggested. Further structural damage was observed as flexural cracking at the column base and beam ends, shear cracking in beam ends and joints, and splitting cracks along the main reinforcement of the beams. Rupture of FRP reinforcement occurred at 5% drift without substantial change in structural response due to a high degree of redundancy in the system.

The findings from previous research activities indicate advantageous structural features of FRP-reinforced concrete, such as high flexural strength, elastic load-deformation behavior, small residual deflections, and small crack widths. They also, however, indicate deficiencies arising from the combination of elastic FRP reinforcement and brittle concrete, most significantly in terms of reinforcement strain distribution in the vicinity of a crack, interfacial bond characteristics, and mode of failure.

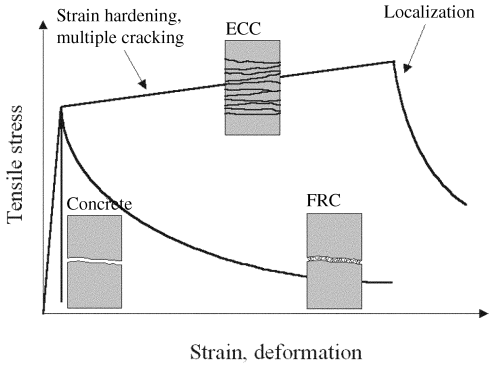


*Fig. 1—Schematic stress-strain behavior of cementitious matrices in tension.*

The present study aims at investigating the effect of elastic stress-strain behavior of FRP reinforcement on the load-deformation behavior of FRP-reinforced engineered cementitious composite (ECC) flexural members under reverse cyclic loading conditions. In this context, the interaction of elastic reinforcement and ductile cementitious matrix with respect to interfacial bond mechanisms, composite damage evolution, member deformation capacity, and failure mode are conceptually outlined, experimentally verified and contrasted to FRP-reinforced concrete. Furthermore, an analytical model for the load-deflection envelope is derived from the moment-curvature relationship and sectional stiffness of the flexural member as a function of applied load.

## RESEARCH SIGNIFICANCE

Research activities presented in this paper are directed at using FRP-reinforced ECC members in seismic resistant structures to reduce residual deflections and prevent inelastic deformations at particular locations while providing relatively large, elastic deflection capacity. These elastic members are expected to be beneficial in controlling the response of structures particularly at large deformations. In contrast to FRP-reinforced concrete, the combination of elastic FRP reinforcement and ductile ECC matrix in these flexural members is expected to result in compatible deformations between reinforcement and matrix, thus effectively decoupling reinforcement stress distribution and flexural crack formation from interfacial bond properties. This study is aimed at investigating these composite deformation mechanisms and their effect on the response of structural members.

### Composite interaction and interfacial bond characteristics

The load-deformation behavior of reinforced concrete members is fundamentally affected by the material properties of reinforcement and cementitious matrix as well as their interaction. The cementitious matrices used in this study, ECC and concrete, differ significantly in their tensile stress-strain behavior. While concrete in tension fails in a brittle manner upon reaching its cracking strength, ECC is designed to undergo a strain-hardening phase analogous to that of metals (Fig. 1). Beyond first cracking, ECC increases its composite tensile stress up to strain levels on the order of several

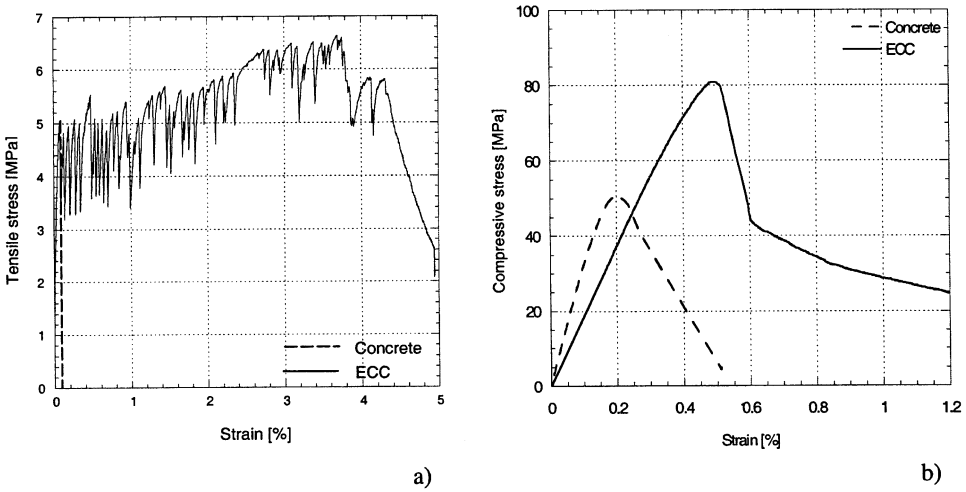


*Fig. 2—Stress-strain behavior of concrete and ECC in: (a) tension; and (b) compression.*

percent (Fig. 2(a)). While concrete and conventional fiber-reinforced concrete (FRC) accommodate imposed tensile deformations by the opening of a discrete crack, ECC shows multiple cracking behavior with small crack spacing (0.5 to 5 mm) and small individual crack widths (< 200 μm). Tensile failure in ECC occurs when the fiber bridging strength at a crack is reached, resulting in localized deformation at this section. The design basis and mechanical properties of ECC are reviewed in detail elsewhere (Li 1998).

In compression, ECC has a lower elastic modulus compared with concrete and reaches its compressive strength at a larger strain due to the lack of large aggregates. The compressive strength of ECC is usually on the order of 30 to 80 MPa, depending on the particular composition. Beyond ultimate, the compressive stress drops to approximately $0.5f_c'$ with subsequently descending stress at further increasing deformation (Fig. 2(b)).

The combination of elastic FRP reinforcement and ductile ECC takes advantage of the material properties of the constituent materials and more importantly of their synergistic interaction. In particular, the interfacial bond mechanism in FRP-reinforced ECC is affected by this interaction, where compatible tensile deformations of reinforcement and matrix on a macroscale prevent relative slip and therefore reduce activation of interfacial bond stress (Fischer and Li 2002a).

Considering an isolated segment from the tensile section of an FRP-reinforced flexural member, prior to formation of flexural cracking the tensile force is proportionally shared between reinforcement and matrix. At formation of an initial flexural crack, the tensile stress in the concrete matrix cannot be directly transferred and is diverted into the reinforcement, resulting in tensile stress concentration and strain discontinuity between concrete and reinforcement. This deformation incompatibility in FRP-reinforced concrete may be accompanied by interfacial bond failure, bond splitting, and/or formation of inclined cracking due to the local stress field in the concrete matrix (Fig. 3(a)).

In contrast, initiation of flexural cracking in the FRP-reinforced ECC member does not result in a stress-free matrix crack, but tensile stress is directly transferred across the crack. Subsequently, ECC enters the strain-hardening regime and stresses are redistributed proportional to the stiffness of reinforcement and matrix at this deformation stage. Although the inelastic stiffness of ECC is significantly lower than in its uncracked state, tensile load in the matrix prior to cracking is

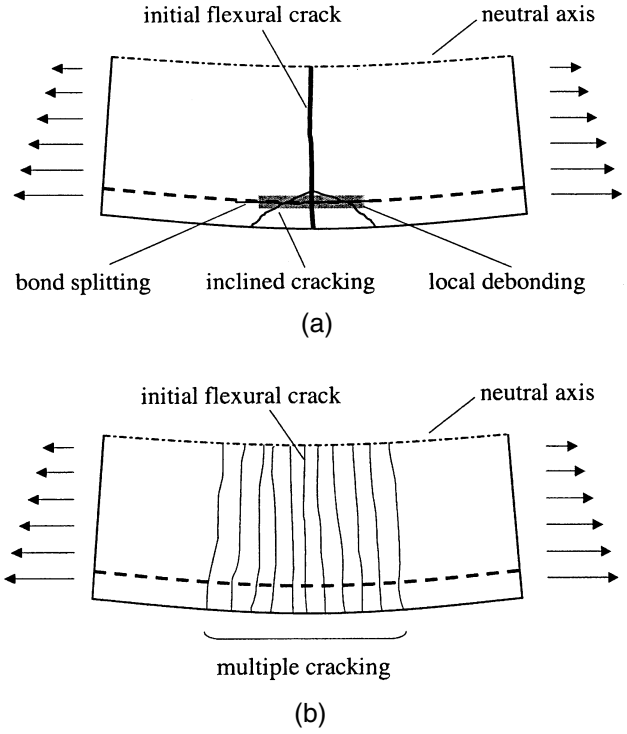


*Fig. 3—Composite deformation mechanism in: (a) FRP-reinforced concrete; and (b) FRP-reinforced ECC.*

transferred by means of fiber bridging and is not diverted into the FRP reinforcement. Due to the uniform stress profile in the cracked matrix, initiation of further flexural cracking is dependent on the tensile deformation characteristics of ECC—that is, multiple cracking width and spacing—and is effectively independent of interfacial bond properties. At increasing flexural load, the induced tensile strains in reinforcement and matrix are accommodated by further elastic deformation in FRP and propagation of multiple cracking in the ECC matrix (Fig. 3(b)). Thus, local stress concentrations in the FRP reinforcement are prevented by direct tensile load transfer in the ECC matrix as well as compatible deformations between reinforcement and matrix. Although fully bonded to the ECC matrix, the unique composite deformation behavior causes a uniform stress distribution in the FRP reinforcement, while maintaining composite action and tension stiffening effect as well as avoiding curvature concentration and excessive

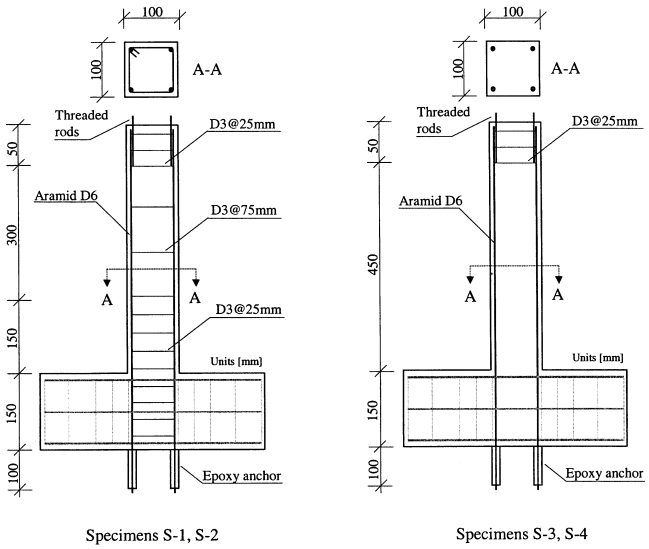


*Fig. 4—Specimen configurations.*

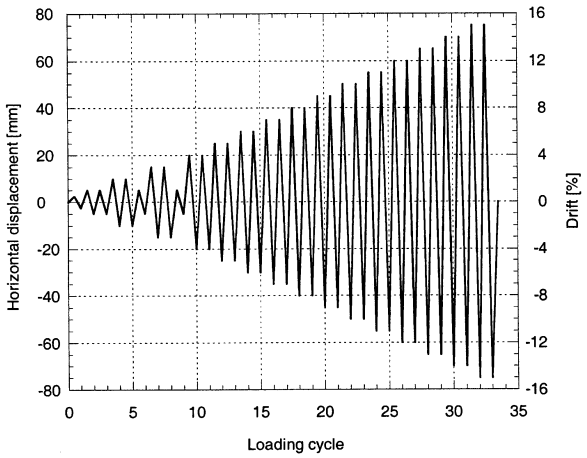


*Fig. 5—Loading sequence.*

compressive stresses in the cementitious matrix above the neutral axis.

This composite deformation mechanism has several implications on the structural performance of FRP reinforced ECC members. The lack of relative slip between reinforcement and ECC in the multiple cracking stage actively prevents interfacial bond deterioration and radial splitting forces. Furthermore, the member deflection capacity is enhanced due to an extended distribution of flexural deformation along the member and thereby reducing peak curvature and sectional strength demands. The inelastic strain capacity of ECC—that is, transition from multiple cracking to localized deformation (Fig. 1)—limits the utilization of the compatible deformation mechanism. At localization, a discrete flexural crack increases in width and interfacial bond stresses are initiated. The confining effect of ECC in the transverse direction, however, is expected to resist bond-splitting forces and prevent spalling of the ECC cover. Therefore, the longitudinal FRP reinforcement is confined and well protected against buckling at all stages of flexural deformation, which is particularly important under alternating tensile and compressive stresses.

### Material composition and properties

The longitudinal reinforcement of the specimens investigated in this study was aramid-FRP commercially available

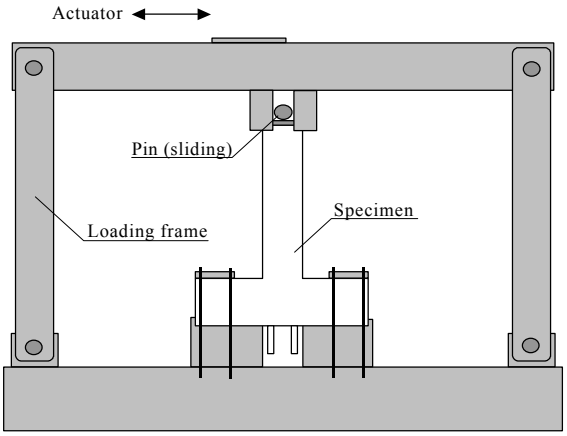


*Fig. 6—Loading configuration.*

by the name of Technora Rod (Teijin Ltd.) with a ribbed surface geometry similar to that of conventional steel reinforcement. The material properties according to the specifications of the manufacturer are a tensile elastic modulus of 54 GPa, an average tensile strength of 1800 MPa, and a tensile strain capacity of 3.8%. In compression, explicit data for this material are not available; however, they are suggested in design guidelines as a compressive strength of approximately 10% of the respective values in tension, that is, 200 MPa at strain of 0.2 to 0.3% (Sonobe, Fukuyama, and Okamoto 1997).

The ECC matrix used 1.5% volume polyethylene fibers, cement, fine aggregates (maximum grain size 0.25 mm), water, high-range water-reducing admixture, and admixtures to enhance the fresh properties of the mixture. Material properties in uniaxial tension obtained from this composition were first cracking strength of 4.5 MPa at 0.01% strain and ultimate tensile strength of 6.0 MPa at approximately 3.8% strain (Fig. 2(a)). The compressive strength of this particular version of ECC was 80 MPa at a strain of 0.5% (Fig. 2(b)).

Concrete used coarse aggregates (maximum grain size 10 mm), cement, water, and high-range water-reducing admixture to enhance the fresh properties of the mixture. Tensile tests on concrete were not conducted but were assumed to have a first cracking strength similar to that of ECC (4.5 MPa at 0.01% strain) and subsequent brittle failure. The compressive strength of concrete used in this study was 50 MPa at a strain of 0.2% (Fig. 2(b)).

## EXPERIMENTAL PROGRAM

### Specimen and loading configuration

The structural behavior of FRP-reinforced ECC flexural members was experimentally investigated and compared to FRP-reinforced concrete using small-scale cantilever beams with 500 mm height and square cross-sectional dimensions of 100 mm (Fig. 4). To provide cantilever-type loading conditions, a rigid transverse beam was integrally cast with the cantilever base. The longitudinal FRP reinforcement was extended through the transverse beam and externally anchored with epoxy-filled steel sleeves (Fig. 4). Lateral loading was applied through a loading frame equipped with a 100 kN capacity actuator according to a displacement-controlled loading sequence (Fig. 5). A steel pin was mounted on top of the cantilever to introduce the lateral load while the transverse beam was fixed to the base of the loading frame (Fig. 6). The loading pin was not restrained in the vertical direction.

The specimens were instrumented with a displacement transducer at the top of the cantilever to measure the total

**Table 1—Summary of specimen configurations**

| Specimen | Composite | Surface | Reinforcement ratio | | Ultimate strength | |
|---|---|---|---|---|---|---|
| | | | $\rho_{longitudinal}$* | $\rho_{transverse}$† | Predicted‡ | Experimental§ |
| S-1 | R/C | Ribbed | 1.13 | 0.57/0.19 | 9.5 | 9.0 |
| S-2 | R/ECC | Ribbed | 1.13 | 0.57/0.19 | 14.2 | 12.5 |
| S-3 | R/ECC | Ribbed | 1.13 | — | 14.2 | 14.3 |
| S-4 | R/ECC | Ribbed, sanded | 1.13 | — | 14.2 | 13.0 |

*Total longitudinal reinforcement ratio, %.
†Transverse reinforcement ratio below $h$ = 150 mm/above $h$ = 150 mm, %.
‡Predicted shear force kN based on 0.003 and 0.006 limit strain in concrete and ECC, respectively.
§Observed shear force kN.

displacement of the specimen. In addition, black-colored dots were spray painted on the surface of the specimen to measure the deflected shape of the specimens by means of an image analysis technique.

This research project involved several types of FRP reinforcement, including aramid, carbon, and polyvinyl alcohol (PVA) FRP, as well as conventional steel reinforcement reported elsewhere (Fischer and Li 2002b). The experimental results presented in this paper focus on specimens reinforced with aramid FRP. The parameters investigated include the type of cementitious matrix (ECC and concrete), transverse reinforcement detailing, and surface coating of the FRP reinforcement.

Results from tests of four different specimen configurations are presented. The specimens were longitudinally reinforced with four FRP bars (∅6 mm) arranged symmetrically relative to both axes (Fig. 4). All specimens were designed so the compressive strength of the cementitious matrix is exceeded prior to rupture of the FRP reinforcement in tension. The experimental tests discussed herein contain a reinforced concrete (RC) control specimen with transverse reinforcement (S-1), a reinforced ECC (R/ECC) specimen with transverse reinforcement (S-2), an R/ECC specimen without transverse reinforcement (S-3), and an R/ECC specimen without transverse reinforcement and additional sand coating (S-4). The details of the specimen configurations are summarized in Table 1.

Transverse reinforcement in Specimens S-1 and S-2 was provided by smooth steel wire (∅3 mm) with 135 degree hooks spaced at 25 mm in the joint region and at the base of the cantilever ($h$ = 150 mm) and at 75 mm spacing above. In all specimens, four threaded rods were placed at the top of the cantilever prior to casting and confined with stirrups (∅3 mm) at 25 mm spacing to mount the loading pin (Fig. 4). The pin was welded to a steel plate, which was then attached to the specimen with an adhesive and additionally tied to the threaded rods.

## EXPERIMENTAL OBSERVATIONS

The load-deformation behavior of the tested specimens was continuously monitored using a data acquisition system. The specimens were visually inspected at each consecutive loading cycle and cracks were marked and crack widths were measured at the tension face of the specimens.

In Specimen S-1 (RC, with transverse reinforcement) flexural cracking initiated at the cantilever base in the first loading cycle (0.5% drift). Individual cracks propagated from the respective tension side extended across the specimen centerline and formed connected crack paths upon load reversal. At 2% drift, only flexural cracking was observed at an approximate spacing of 100 mm and maximum crack width of 1mm on the tension face near the base of the specimen. At further

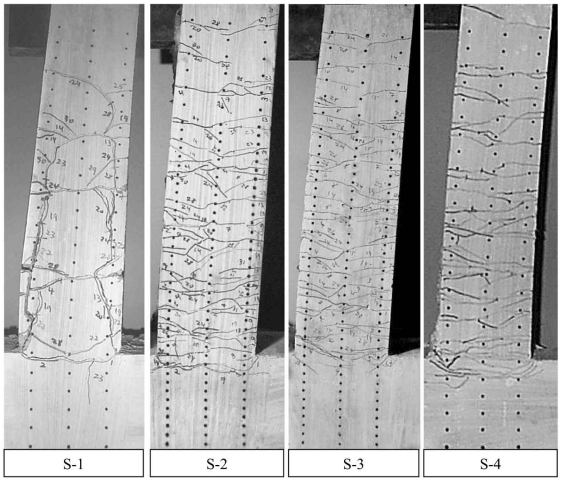


*Fig. 7—Deflected shape and damage pattern of specimens at 7% drift.*

increasing drift levels, the number of flexural cracks slightly increased and extended up to 350 mm specimen height with a maximum crack opening of 2 mm at the cantilever base. Additional cracks initiating at the intersection of existing flexural cracks and position of longitudinal reinforcement became apparent at 5% drift and partly extended at a 45 degree angle towards the tension side as well as propagated along the FRP reinforcement as bond splitting cracks. These longitudinal splitting cracks further developed under the influence of compressive stress in the reverse half-cycle and led to extensive debonding along 250 mm specimen height followed by minor crushing and detachment of cover concrete at 6% drift. Damage propagation coincided with increasing nonlinearity of the load-deformation response and near complete loss of flexural stiffness at 7% drift. Due to further crushing of concrete in the initial half-cycle at 7% drift (Fig. 7), the longitudinal FRP reinforcement presumably experienced excessive compressive strain and subsequently failed by partial tendon rupture tension in the reverse half-cycle at an applied shear force of 9 kN.

In Specimen S-2 (R/ECC, with transverse reinforcement), flexural cracking formed during the initial loading cycles and at 2% drift extended up to 300 mm specimen height with an approximate crack spacing of 40 mm and maximum crack width of 0.1 mm. The number of flexural cracks increased significantly up to 5% drift with crack formation up to 400 mm specimen height. The average crack spacing reduced to 20 mm with a maximum crack opening of 0.2 mm at the cantilever base. The inclination of cracking indicates predominant flexural deformation; however, few minor shear cracks formed particularly in the midsection of the cantilever. At

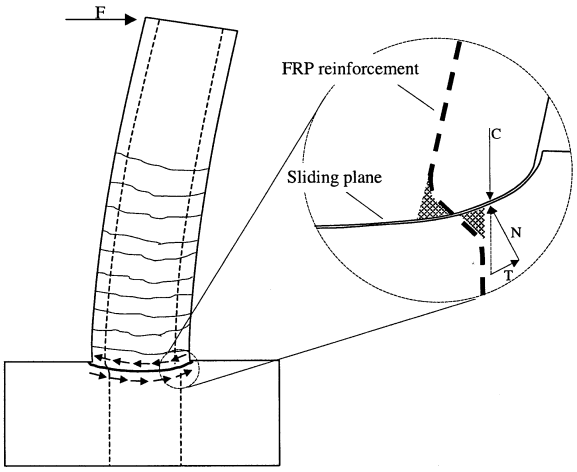


*Fig. 8—Rotational sliding mechanism and local damage to FRP reinforcement.*

this loading stage, neither localization of flexural cracking nor bond splitting cracks were observed.

The number of flexural cracks stabilized at 6% drift and cracking localized at the cantilever base. Although a number of additional cracks formed throughout the specimen up to 450 mm height, predominantly extending at a 45 degree angle and interconnecting already existing cracks, shear failure was not observed. Beyond 7% drift, a tendency of rotational sliding and grinding between the specimen foundation and cantilever section along an interconnected flexural crack plane became apparent (Fig. 8), while only minor crushing of ECC was observed. Tensile rupture of FRP reinforcement in Specimen S-2 occurred at this sliding plane at 12% drift and an applied shear force of 13 kN.

The deformation behavior of Specimen S-3 (R/ECC, without transverse reinforcement) was very similar to that of Specimen S-2; however, the distribution of flexural cracking was more uniform with an average spacing of 15 mm and less significant shear crack formation. Localization of cracking occurred at 7% drift with flexural cracks extending up to 400 mm cantilever height. Crushing of ECC cover was observed at 8% drift, while rotational sliding was less significant. Ultimate failure of Specimen S-3 occurred by rupture of FRP at 13% drift and an applied shear force of 14 kN.

The deformation behavior of Specimen S-4 (R/ECC, without transverse reinforcement, sand coating) was generally similar to Specimens S-2 and S-3. Even though the ultimate crack spacing was comparable to that of Specimen S-3 (15 mm), a concentration of flexural cracking was observed at the cantilever base, while at deflections up to 7% drift the number of cracks above the cantilever base was slightly smaller compared with S-2 and S-3. Localization of cracking was delayed beyond 7% drift and flexural cracks continuously initiated up to 10% drift and extended to 400 mm cantilever height. Crushing of ECC and rotational sliding occurred beyond 10% drift accompanied by a decrease in shear force. Ultimately, Specimen S-4 failed by FRP-reinforcement rupture at 13% drift and applied shear force of 12.5 kN.

## DISCUSSION

The load-deformation response of the tested specimens, FRP-reinforced concrete as well as FRP reinforced ECC, is predominantly characterized by nonlinear elastic behavior with relatively small residual deflections. As intended, failure is initiated by inelastic deformations of concrete in Specimen S-1 and ECC in Specimens S-2, S-3, and S-4. Ultimate failure occurred in all considered cases by reinforcement rupture due to reverse cyclic loading conditions and resulting damage on the longitudinal reinforcement under compression.

The apparent differences between FRP-reinforced concrete and FRP-reinforced ECC in terms of load-deformation response, damage evolution, and deflection capacity are established in detail by comparing Specimens S-1 and S-2. Furthermore, the behavior of Specimens S-3 and S-4 is compared to Specimen S-2 to investigate the influence of reinforcement detailing and interfacial bond properties on FRP-reinforced ECC members.

### Load-deformation response

Flexural cracking in Specimens S-1 (RC with transverse reinforcement) and S-2 (R/ECC with transverse reinforcement) occurred as predicted at relatively small flexural loads and deflections, which are for all practical purposes insignificant compared to service and ultimate deflections. In Specimen S-1 (Fig. 9(a)), crack initiation resulted in a load drop and temporary instability as the deflection increased without additional loading due to the transition between uncracked and cracked sectional moment of inertia and load transfer from concrete to FRP reinforcement. In contrast, the formation of flexural cracking in Specimen S-2 (Fig. 9(b)) causes a change in flexural stiffness; however, a significant load drop and simultaneous deflection increase are not apparent in the load-deformation response, which is attributed to the direct load transfer in the cracked ECC matrix.

Beyond initiation of flexural cracking and at increasing drift levels, the formation of further flexural cracks is limited in Specimen S-1 due to interfacial bond properties and load transfer length between FRP reinforcement and concrete, resulting in a relatively large crack spacing of approximately 100 mm (Fig. 7). Therefore, imposed specimen deflections are accommodated by relatively large crack widths. The crack spacing in Specimen S-2 is significantly smaller at all drift levels (Fig. 7) especially at the cantilever base and similar to the crack spacing observed in this particular version of ECC in direct tension (10 mm), suggesting that flexural crack formation is effectively independent of the interaction with the FRP reinforcement. The formation of bond-splitting cracks in Specimen S-1 and the lack thereof in Specimen S-2 further indicate differences in the respective composite deformation mechanism. While the strain lag between reinforcement and concrete at a crack location causes relative slip and radial stresses exceeding the matrix tensile strength as indicated by significant formation of bond splitting cracks, compatible deformations between reinforcement and ECC in the multiple cracking stage prevent significant bond stress and relative slip.

At further increasing deflection, the load-deformation behavior of Specimens S-1 and S-2 is characterized by a progressive reduction of flexural stiffness at increasing applied load. A strictly linear portion of the response cannot be clearly identified, which is due to inelastic deformations in the cementitious matrices in tension and compression. These inelastic deformations initially result from successive formation of flexural cracking; however, beyond flexural crack saturation they are dominated by nonlinear deformation of the cementitious matrices in compression. Furthermore, progressing interfacial bond failure and bond splitting-cracks in Specimen S-1 contribute to stiffness reduction and increasing nonlinearity of the load-deformation response. Disintegration of the FRP-reinforced concrete composite by

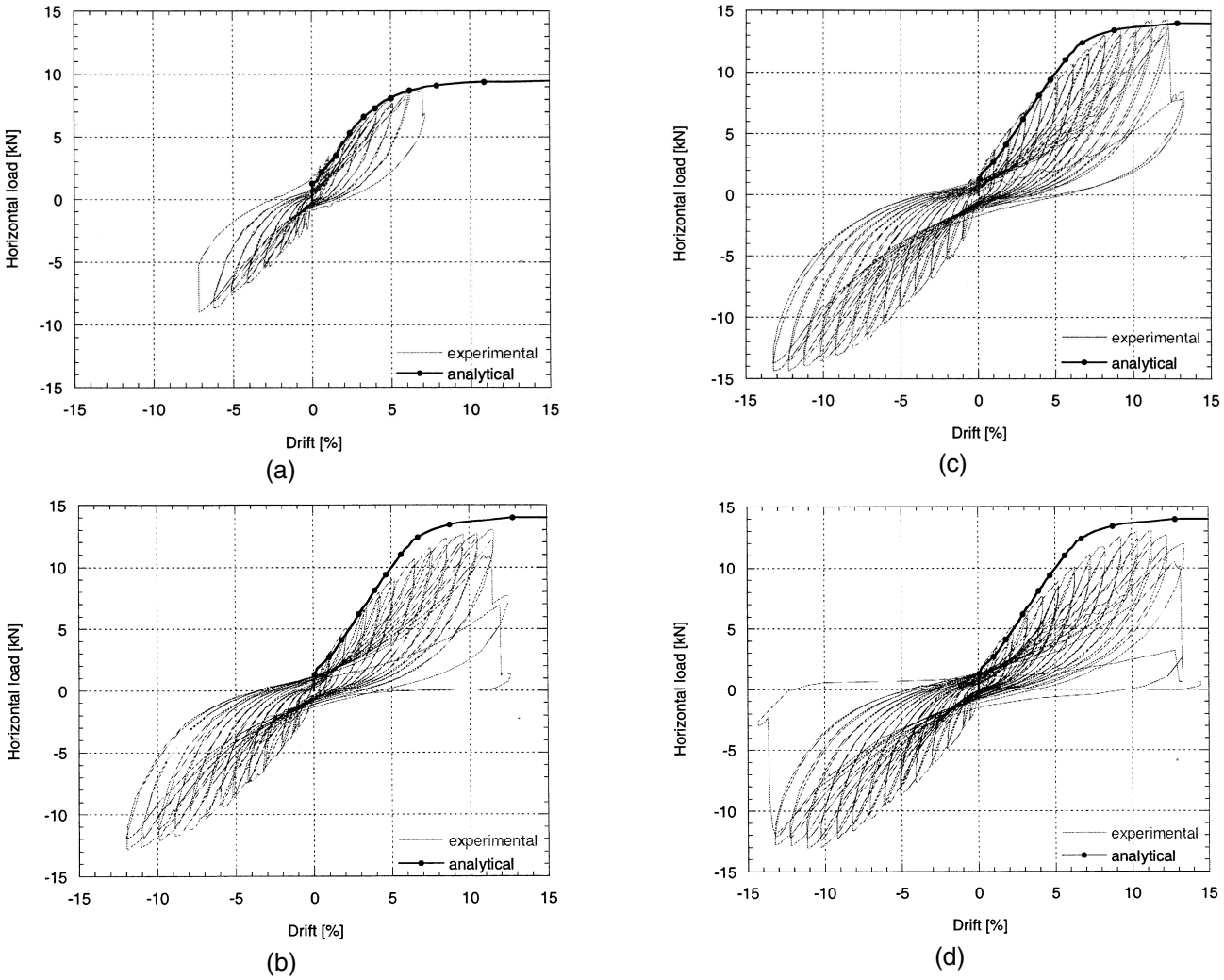


*Fig. 9—Load-deformation behavior of: (a) Specimen S-1 (R/C with transverse reinforcement); (b) Specimen S-2 (R/ECC with transverse reinforcement); (c) Specimen S-3 (R/ECC without transverse reinforcement); and (d) Specimen S-4 (R/ECC without transverse reinforcement, sand coating).*

crushing and bond splitting induces severe damage to the FRP reinforcement and partial rupture occurs at 7% drift and ultimate load of approximately 9 kN. Although the experimentally obtained flexural strength is in satisfactory agreement with predicted values based on a maximum compressive strain of 0.003 in concrete, the nominal stress in the reinforcement at rupture is well below its nominal tensile strength, which indicates the effect of damage-induced strength reduction in the FRP reinforcement.

In Specimen S-2, flexural cracking continuously initiates up to relatively large deflections (7% drift), beyond which flexural stiffness reduction is influenced by ECC crushing and primarily rotational sliding at the cantilever base (Fig. 8). The transition between these phases is indicated by a noticeable plateau in the load-deformation curve beyond 7% drift (Fig. 9(b)). Ultimately, rotational sliding of ECC as well as crushing lead to tensile rupture of the FRP reinforcement at 12% drift and ultimate shear force of approximately 13 kN. Similar to Specimen S-1, the nominal tensile strength of the reinforcement is not exceeded at this point; however, damage induced by compressive and transverse deformations considerably reduces the tensile capacity.

## Curvature distribution

Information on the sectional contribution to total cantilever deflection is obtained by analyzing digital images taken of the specimens at reaching the target displacement at each drift level. These images are processed using computer software and the coordinates of dots painted on the specimen surface are obtained. These coordinates represent the deflected shape of the specimen at a given drift level, which is then used to derive the deflection angle and curvature distribution along the specimen. The resolution of the camera (1520 x 960 pixels) permits deformation measurements with an accuracy of approximately 0.5 mm at given dimensions of the specimen.

The curvature distribution of Specimens S-1 (Fig. 10(a)) and S-2 (Fig. 10(b)) is plotted at increasing drift levels at positions between the joint region and 250 mm specimen height. Data obtained at positions above 250 mm are predominantly influenced by error due to the minute curvature at these sections and limited resolution of the digital images. The curvature distribution in both specimens indicates elastic behavior with gradually decreasing curvature along the cantilever as opposed to curvature concentration at the base, which is typical for steel-reinforced members in the inelastic deformation regime (Fischer and Li 2002b).

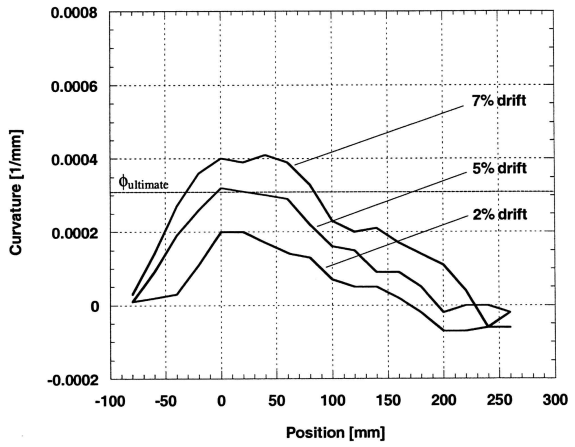


(a)

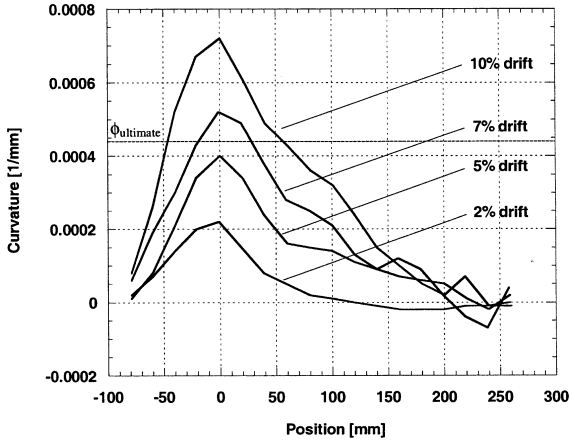


(b)

*Fig. 10—Curvature distribution in: (a) Specimen S-1 (R/C, transverse reinforcement); and (b) Specimen S-2 (R/ECC, transverse reinforcement).*

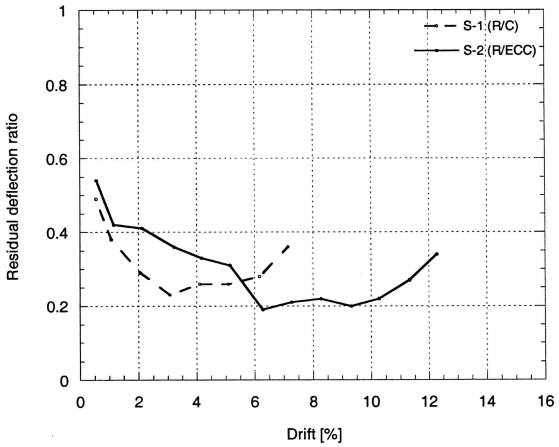


*Fig. 11—Residual deflection of Specimens S-1 and S-2.*

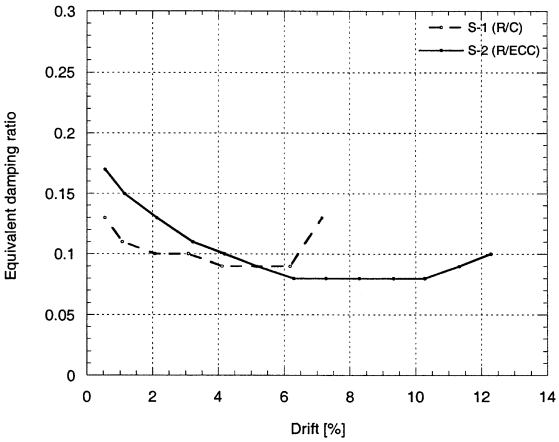


*Fig. 12—Equivalent damping of Specimens S-1 and S-2.*

At 2% drift, the maximum curvature at the cantilever base is similar in both specimens (0.0002 1/mm). In Specimen S-1, the curvature gradually decreases towards the top of the cantilever, while in Specimen S-2 it descends more rapidly. This difference is more pronounced at 5 and 7% drift when the curvature in the FRP-reinforced concrete composite remains nearly constant between the cantilever base and approximately 60 mm height. The variation of curvature along the height of the specimen is influenced by the moment distribution and sectional stiffness of the specimen. Therefore, a constant curvature in Specimen S-1 suggests invariable stress distribution in the FRP reinforcement at these sections caused by debonding and detachment of concrete surrounding the reinforcement. In contrast, the curvature distribution in Specimen S-2 maintains a descending slope at all drift levels particularly at the base due to preserved composite integrity and mechanical interaction between elastic FRP reinforcement and ECC matrix.

Peak curvature in Specimen S-1 was measured at approximately 0.00040 1/mm prior to failure at 7% drift, which slightly exceeds the ultimate curvature $\phi_{ultimate}$ of 0.00031 1/mm obtained from the theoretical moment-curvature relationship. Similarly, the measured peak curvature in Specimen S-2 (0.00072 1/mm) significantly exceeds the predicted value (0.00044 1/mm) at ultimate. This discrepancy may be caused by actual strain capacities of the cementitious matrices beyond those assumed in the moment-curvature relationship (0.003 in concrete, 0.006 in ECC), possibly due to confinement effects of the transverse reinforcement.

## Residual deflection and energy dissipation

The behavior of Specimens S-1 and S-2 in terms of residual deflection (Fig. 11) and energy dissipation (Fig. 12) is compared at increasing drift levels. In this study, residual deflection is characterized by the ratio of permanent deflection after unloading and maximum deflection experienced at a given drift level. Energy dissipation is represented by the equivalent damping ratio, defined as the energy dissipated during a complete loading cycle normalized by the elastic energy stored in the member at a given drift level (Chopra 1995).

Flexural crack formation primarily affects the specimen behavior at small drift levels in terms of residual deflection and energy dissipation. Incomplete crack closure after unloading at small drift levels significantly contributes to the residual deflection of Specimens S-1 and S-2, which show relatively large residual deflection ratios at 0.5% drift. At increasing drift levels, this ratio declines in both specimens and reaches a minimum of approximately 0.2, however at different drift levels. Minimum residual deflection in S-1 is observed at 3% drift and in S-2 at 6% drift, which roughly coincides with flexural crack saturation in both specimens, respectively. In Specimen S-1, additional inelastic deformation mechanisms, such as bond splitting, spalling, and compression failure, succeed this phase particularly beyond 5% drift, thus the

residual deflection ratio increases rapidly. In Specimen S-2, flexural crack saturation is achieved at approximately 7% drift, beyond which the residual deflection ratio remains constant at 0.2 due to a stable flexural deformation mechanism. At deflections above 10% drift, crushing of ECC and rotational sliding constitute a major change in the deformation mechanism, resulting in a considerable increase in residual deflection ratio.

The energy dissipation characteristics of both specimens show trends very similar to those described for the residual deflection ratio. In both specimens, S-1 and S-2, the formation of flexural cracking is affecting the residual deflections as well as the equivalent damping characteristics, which reach their respective minimum at flexural crack saturation. At increasing deflections beyond flexural crack saturation, the residual deflection ratio and equivalent damping ratio remain constant due to internal friction along the flexural crack planes. Ultimately, damage by matrix crushing, spalling, and rotational sliding results in a slight increase in residual deflections and equivalent damping.

These observations suggest that flexural crack formation and saturation as well as damage induced by compression have a major influence on residual deflection and equivalent damping characteristics of FRP-reinforced members. While at drift levels prior to flexural crack saturation, FRP-reinforced ECC (S-2) shows larger residual deflection due to the larger number of flexural cracks compared with FRP-reinforced concrete (S-1); it is able to maintain its flexural deformation mode beyond saturation with small residual deflections up to relatively large drift levels.

### Transverse reinforcement

The comparison of Specimen S-2 (R/ECC with transverse reinforcement) (Fig. 9(b)) and S-3 (R/ECC without transverse reinforcement) (Fig. 9(c)) indicates higher ultimate strength and deflection of Specimen S-3 without transverse reinforcement. In view of identical longitudinal reinforcement in both specimens, this suggests that the presence of stirrups in Specimen S-2 contributes to tensile strength reduction in the FRP reinforcement leading to premature failure. Inspection of Specimen S-2 after completion of the test gives evidence supporting this assumption. Rupture of FRP exclusively occurred at the intersection with stirrups, which locally constrained and punctured the longitudinal reinforcement. The experimentally obtained flexural strength of Specimen S-3 is nearly identical to that predicted and, therefore, its ultimate strength is considered optimal at given material properties of reinforcement and matrix. Lateral support and confinement of FRP reinforcement in S-3 is entirely provided by ECC. In contrast to a discrete lateral support in members with conventional stirrups, the longitudinal reinforcement is continuously supported, confined, and protected in the ECC matrix without intermittent restraint. The comparison of Specimens S-2 and S-3 suggests that transverse reinforcement should not be used in FRP-reinforced ECC flexural members if shear strength requirements permit. Although transverse reinforcement is usually found to enhance effective compressive strength and strain capacity of cementitious materials (concrete, ECC), which is advantageous in compression-controlled members, its damaging effect on FRP reinforcement is detrimental. From the experimental results obtained in this study, it is found that the self-confining effect of ECC is sufficient to prevent reinforcement buckling and assure ductile compressive failure so that additional confinement reinforcement is not necessary.

In addition, the shear capacity of ECC satisfies strength requirements to prevent premature shear failure for the given specimen configuration. The predominant formation of flexural cracks in specimens using ECC leaves the transverse reinforcement largely ineffective due to its orientation parallel to the flexural cracks. Furthermore, the absence of stirrups is found to enhance flexural crack formation, as it does not obstruct a random orientation of fibers in the ECC matrix particularly at the cantilever base.

### Interfacial bond strength

The modification of the FRP reinforcement surface by additional sand coating does not positively affect the load-deformation behavior of Specimen S-4 (R/ECC without transverse reinforcement, sand coating) (Fig. 9(d)) compared with S-3 (R/ECC without transverse reinforcement) (Fig. 9(c)). Maximum crack widths are identical prior to localization of cracking and, ultimately, flexural crack spacing and distribution are similar in both specimens; however, in Specimen S-4, local crack spacing at the cantilever base is found slightly smaller and localization of cracking is to some extent delayed. The increased crack density at the cantilever base weakens the compressive strength of the matrix and promotes the formation of a rotational sliding plane, which negatively affects flexural stiffness and strength of Specimen S-4.

The comparison of Specimens S-3 and S-4 with respect to load-deformation behavior and flexural crack formation confirms the assumption that the composite deformation characteristics of reinforced ECC members are effectively independent of the interfacial bond properties, provided that sufficient development length is available or external anchorage is supplied. Further details on the effect of additional surface coating with respect to reinforcement strain distribution cannot be reliably derived from the experimental data obtained in this study.

### Analytical load-deflection relationship

In this study, the model for the load-deflection envelope is fundamentally based on the theoretical moment-curvature relationship, which is derived from material properties of the FRP reinforcement in tension and the cementitious matrices in compression. From this relationship, the stiffness of the cracked sections of the member is determined as a function of maximum moment and subsequently used for the derivation of the load-deflection envelope. Although the stress-strain behavior of ECC indicates considerable tensile strength in the inelastic deformation regime, its direct effect on the load-deformation behavior of the FRP-reinforced ECC members is found insignificant and therefore the tensile contribution of both matrices used in this study are neglected in the analysis. These assumptions may lead to conservative estimates under monotonic loading conditions; however, inelastic tensile deformations of fiber-reinforced composites in general and ECC in particular are usually accommodated by unrepeatable mechanisms such as fiber debonding and pullout, which cannot be reversed and repeatedly used.

The relevant material properties of the FRP reinforcement are the tensile elastic modulus (54 GPa) and ultimate strength (1800 MPa). The compressive stress-strain behavior of concrete and ECC are characterized by a parabola prior to reaching peak stress and linearly descending tail (Hognestad 1955). Based on these parameters, the moment-curvature relationships of Specimen S-1 and Specimen S-2 (S-3, S-4 with identical section properties) are constructed using a conventional spreadsheet program (Fig. 13). For both specimens,

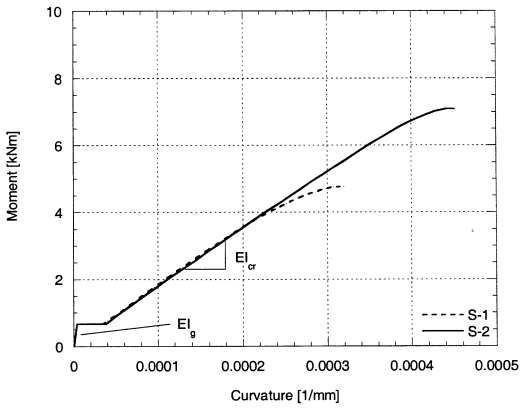


*Fig. 13—Moment-curvature relationships of Specimens S-1 and S-2.*

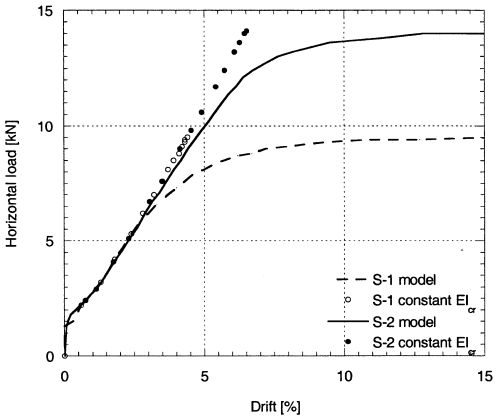


*Fig. 14—Theoretical load-deflection relationships of Specimens S-1 and S-2.*

the respective uncracked sectional stiffness ($EI_g$) is approximated neglecting the presence of the FRP reinforcement and the cracked sectional stiffness ($EI_{cr}$) at increasing moment is taken directly from the moment-curvature diagram.

The total deflection $\Delta(x = L)$ of the specimen is obtained by integrating the curvature partially over the cracked length with sectional stiffness $EI_{cr}$ at given applied load and partially over the uncracked length with sectional stiffness $EI_g$. After consideration of the boundary conditions of each segment and assuming a constant sectional stiffness $EI_{cr}$ along the cracked length $l_{cr}$ at a given load and $EI_g$ along the uncracked length of the cantilever, the derivation of cantilever deflection $\Delta$ as a function of applied lateral load $F$ leads to

$$\Delta(x = L) = \frac{F}{EI_{cr}}\left(\frac{1}{2}Ll_{cr}^2 - \frac{1}{6}l_{cr}^3\right) + \frac{F}{EI_{cr}}\left(Ll_{cr} - \frac{1}{2}l_{cr}^2\right)$$

$$(L - l_{cr}) + \frac{F}{3EI_g}(L - l_{cr})^3$$

In this expression, the first term represents the deflection at the end of the cracked length of the cantilever, the second term represents the geometric deflection of the uncracked length due to the rotation angle at the boundary between cracked and uncracked length, and the third term represents the elastic deflection of the uncracked length.

To account for a varying sectional stiffness $EI_{cr}$ depending on the magnitude of applied load—that is, slope of the moment-curvature diagram at a maximum moment corresponding to the applied load—a numerical procedure is used to represent the aforementioned relationship.

In all specimens, the theoretical solution slightly overestimates specimen deflections in the initial loading cycle at small-to-moderate drift levels, due to the initial tensile contribution of the cementitious matrices. In the reloading cycle, however, experimental results and analytical solution agree because the tensile contribution of concrete is lost beyond crack formation and in ECC is inactive below previously experienced deformation levels.

In Specimen S-1, experimental data and theoretical solution agree in the elastic and inelastic deformation regime. Although Specimens S-2, S-3, and S-4 have the same cross-sectional properties, their load-deformation behavior is different. Satisfactory agreement with the theoretical solution is obtained only in Specimen S-3, while the response of Specimens S-2 and S-4 departs considerably from the prediction at moderate and large drift levels. This difference may be due to physical mechanisms not considered in the model, specifically rotational sliding, which is more evident in Specimens S-2 and S-4 and may lead to lower flexural stiffness and premature rupture of the FRP reinforcement.

In another approach (Razaqpur, Švecová, and Cheung 2000), the neutral axis position was assumed constant under service load conditions, implying elastic matrix deformation and a constant cracked sectional stiffness $EI_{cr}$ independent of applied load and resulting in a model valid only under service load conditions (Fig. 14). In this study, $EI_{cr}$ is derived from the moment-curvature relationship, which is found through an iterative procedure at increasing matrix compressive strain and accounts for inelastic deformation of the cementitious matrix. Therefore, the model for the load-deflection envelope is applicable beyond service load conditions up to failure by crushing of the cementitious matrix (Fig. 14). Both models agree in the elastic deformation regime of the cementitious matrices however differ significantly above $0.7P_u$ for Specimen S-1 and $0.5P_u$ for Specimen S-2, coinciding with inelastic deformations of concrete and ECC, respectively.

The model suggested in this study is able to capture the influence of inelastic deformation of the cementitious matrices however cannot predict ultimate deformations induced by rupture of the reinforcement because its nominal strength is not exceeded. This effect could be incorporated by tensile strength reduction of the FRP reinforcement depending on the compressive strain experienced in the loading history.

## CONCLUSIONS

The performance of FRP-reinforced flexural members under reversed cyclic loading conditions indicates nonlinear elastic load-deformation behavior with relatively small residual deflections. While the overall load-deformation behavior of FRP-reinforced concrete and ECC shows similarities, detailed differences are established in terms of their composite deformation mechanism, damage evolution, and ultimate deflection capacity.

Deformation compatibility between FRP reinforcement and ECC is found to effectively eliminate interfacial bond stress and relative slip in the multiple cracking deformation regime, preventing bond splitting and spalling of ECC cover. In contrast, incompatible deformations between reinforcement and concrete cause a loss of interfacial bond and composite action resulting in damage to the reinforcement and limited deflection capacity of the FRP-reinforced concrete member.

While the increased flexural strength of FRP-reinforced ECC compared to reinforced concrete is mainly attributed to the compressive strength of ECC, the deflection capacity is fundamentally affected by improved composite interaction. The load-deformation response of FRP-reinforced ECC is dominated by flexural deformation up to relatively large drift levels and crack formation is found effectively independent of interfacial bond properties. Inelastic deformation of ECC in compression leads to flexural stiffness reduction and ultimately gradual mode of failure; however, it also induces compressive strain and tensile strength reduction in the FRP reinforcement.

Despite the ductile deformation behavior of ECC in direct tension, FRP-reinforced ECC members do not have significant energy absorption capacity compared with conventional steel-reinforced members. Flexural crack formation is the primary dissipating mechanism and, therefore, cannot be repeatedly used.

The load-deformation response of the tested specimens is modeled based on the sectional moment-curvature relationship, considering inelastic deformation of the cementitious matrix and its influence on the stiffness of a cracked section. The model is in reasonable agreement with the experimental response however cannot incorporate the effect of rotational sliding, which in some cases has significant influence on flexural stiffness and strength.

## ACKNOWLEDGMENTS

The research described in this paper has been supported by a grant from the National Science Foundation (CMS-0070035) to the ACE-MRL at the University of Michigan. This support is gratefully acknowledged.

## NOTATION

$E$ = modulus of elasticity of cementitious matrix
$F$ = applied load at cantilever
$I_{cr}$ = moment of inertia (cracked)
$I_g$ = moment of inertia (uncracked)
$L$ = length of cantilever
$l_{cr}$ = length of cracked section
$\Delta$ = deflection of cantilever

## REFERENCES

ACI Committee 440, 1996, "State-of-the-Art Report on Fiber Reinforced Plastic (FRP) Reinforcement for Concrete Structures (440R-96)," American Concrete Institute, Farmington Hills, Mich., 65 pp.

Alsayed, S. H., 1998, "Flexural Behavior of Concrete Beams Reinforced with GFRP Bars," *Cement and Concrete Composites*, V. 20, Elsevier Science Ltd., pp. 1-11.

Alsayed, S. H., and Alhozaimy, A. M., 1999, "Ductility of Concrete Beams Reinforced with FRP Bars and Steel Fibers," *Journal of Composite Materials*, V. 33, No. 19, pp. 1792-1806.

Benmokrane, B.; Chaalal, O.; and Masmoudi, R., 1996, "Flexural Response of Concrete Beams Reinforced with FRP Reinforcing Bars," *ACI Materials Journal*, V. 91, No. 2, May-June, pp. 46-55.

Benmokrane, B.; Theriault, M.; Masmoudi, R.; and Rizkalla, S., 1997, "Effect of Reinforcement Ratio on Concrete Members Reinforced with FRP Bars," *Proceedings of the 42nd International SAMPE Symposium*, pp. 87-98.

Burgoyne, C. J., 1993, "Should Fiber Reinforced Plastic be Bonded to Concrete?," *Fiber Reinforced Plastic Reinforcement for Concrete Structures*, SP-138, A. Nanni and C. W. Dolan, eds., American Concrete Institute, Farmington Hills, Mich., pp. 367-380.

Chopra, A. K., 1995, *Dynamics of Structures—Theory and Applications to Earthquake Engineering*, Prentice-Hall, Inc., pp. 94-100.

Cosenza, E.; Manfredi, G.; and Realfonzo, R., 1997, "Behavior and Modeling of Bond of FRP Rebars to Concrete," *ASCE Journal of Composites for Construction*, V. 1, No. 2, May, pp. 40-51.

El-Sheikh, M. T.; Sause, R.; and Pessiki, S., 1999, "Seismic Behavior and Design of Unbonded Post-Tensioned Precast Concrete Frames," *PCI Journal*, May-June, pp. 54-71.

Fischer, G., and Li, V. C., 2002a, "Influence of Matrix Ductility on the Tension-Stiffening Behavior of Steel Reinforced Engineered Cementitious Composites (ECC)," *ACI Structural Journal*, V. 99, No. 1, Jan.-Feb., pp. 104-111.

Fischer, G., and Li, V. C., 2002b, "Effect of Matrix Ductility on Deformation Behavior of Steel-Reinforced ECC Flexural Members under Reversed Cyclic Loading Conditions," *ACI Structural Journal*, V. 99, No. 6, Nov.-Dec., pp. 781-790.

Focacci, F.; Nanni, A.; and Bakis, C. E., 2000, "Local Bond-Slip Relationship for FRP Reinforcement in Concrete," *ASCE Journal of Composites for Construction*, V. 4, No. 1, Feb., pp. 24-31.

Fukuyama, H.; Masuda, Y.; Sonobe, Y.; and Tanigaki, M., 1995, "Structural Performances of Concrete Frame Reinforced with FRP Reinforcement," *Non-Metallic (FRP) Reinforcement for Concrete Structures*, Proceedings of the Second International RILEM Symposium (FRPRCS-2), E&FN Spon, London, pp. 275-286.

Guo, J., and Cox, J. V., 2000, "An Interface Model for the Mechanical Interaction Between FRP Bars and Concrete," *Journal of Reinforced Plastics and Composites*, V. 19, No. 1, pp. 15-33.

Harris, H. G.; Samboonsong, W.; and Ko, F. K., 1998, "New Ductile FRP Reinforcing Bar for Concrete Structures," *ASCE Journal for Composites for Construction*, V. 2, No. 1, Feb., pp. 28-37.

Hognestad, E.; Hansen, N. M.; and McHenry, D., 1955, "Concrete Stress Distribution in Ultimate Strength Design," ACI JOURNAL, *Proceedings* V. 52, pp. 455-479.

Katz, A., 2000, "Bond to Concrete of FRP Rebars after Cyclic Loading," *ASCE Journal of Composites for Construction*, V. 4, No. 3, Aug., pp. 137-144.

Kurama, Y.; Pessiki, S.; and Sause, R., 1999, "Seismic Behavior and Design of Unbonded Post-Tensioned Precast Concrete Walls," *PCI Journal*, May-June, pp. 72-89.

Lees, J. M., and Burgoyne, C. J., 1999, "Experimental Study of Influence of Bond on Flexural Behavior of Concrete Beams Pretensioned with Aramid Fiber Reinforced Plastics," *ACI Structural Journal*, V. 96, No. 3, May-June, pp. 377-385.

Li, V. C., 1998, "Engineered Cementitious Composites—Tailored Composites Through Micromechanical Modeling," *Fiber Reinforced Concrete: Present and the Future*, N. Banthia, A. Bentur, A. and A. Mufti, eds., Canadian Society for Civil Engineering, Montreal, Canada, pp. 64-97.

Naaman, A. E., and Jeong, S. M., 1995, "Structural Ductility of Concrete Beams Prestressed with FRP Tendons," *Non-Metallic (FRP) Reinforcement for Concrete Structures*, Proceedings of the Second International RILEM Symposium (FRPRCS-2), E&FN Spon, London.

Nanni, A., 1993, "Flexural Behavior and Design of RC Members using FRP Reinforcement," *ASCE Journal of Structural Engineering*, V. 119, No. 11, Nov. 1993, pp. 3344-3359.

Nanni, A., and Taginaki, M., 1992, "Pretensioned Prestressed Concrete Members with Bonded Fiber-Reinforced Plastic Tendons: Development and Flexural Bond Length (Static)," *ACI Structural Journal*, V. 89, No. 4, July-Aug., pp. 433-441.

Pecce, M.; Manfredi, G.; and Cosenza, E., 2000, "Experimental Response and Code Models of GFRP RC Beams in Bending," *ASCE Journal of Composites for Construction*, V. 4, No. 4, Nov., pp. 182-190.

Priestley, M. J. N.; Sritharan, S. S.; and Conley, J. R., 1999, "Preliminary Results and Conclusions from PRESSS Five-Story Precast Concrete Test Building," *PCI Journal*, Nov.-Dec., pp. 42-67.

Razaqpur, A. G.; Švecová, D.; and Cheung, M. S., 2000, "Rational Method for Calculating Deflection of Fiber-Reinforced Polymer Reinforced Beams," *ACI Structural Journal*, V. 97, No. 1, Jan.-Feb., pp. 175-184.

Ricles, J. M.; Sause, R.; and Garlock, M. M., 2001, "Posttensioned Seismic Resistant Connections for Steel Frames," *ASCE Journal of Structural Engineering*, V. 127, No. 2, Feb., pp. 113-121.

Sonobe, Y.; Fukuyama, H.; and Okamoto, T., 1997, "Design Guidelines of FRP Reinforced Concrete Building Structures," *ASCE Journal of Composites for Construction*, V. 1, No. 3, Aug. 1997, pp. 90-115.

Taerwe, L., ed., 1995, "Non-Metallic (FRP) Reinforcement for Concrete Structures," *Proceedings of the Second International RILEM Symposium (FRPRCS-2)*, E&FN Spon, London.

Theriault, M., and Benmokrane, B., 1998, "Effects of FRP Reinforcement Ratio and Concrete Strength on Flexural Behavior of Concrete Beams," *ASCE Journal of Composites for Construction*, V. 2, No. 1, Feb., pp. 7-15.

Tighiouart, B.; Benmokrane, B.; and Gao, D., 1998, "Investigation of Bond in Concrete Member with Fiber Reinforced Polymer (FRP) Bars," *Construction and Building Materials*, V. 12, No. 8, Dec., pp. 453-462.

Ye, J. Q., and Wu, Z. J., 2000, "Micro-Mechanical Analysis of Splitting Failure in Concrete Reinforced with Fiber Reinforced Plastic Rods," *Cement and Concrete Composites*, V. 22, No. 4, Aug., pp. 243-251.

Yost, J. R.; Goodspeed, C. H.; and Schmeckpeper, E. R., 2001, "Flexural Performance of Concrete Beams Reinforced with FRP Grids," *ASCE Journal of Composites for Construction*, V. 5, No. 1, Feb., pp. 18-25.